Excited state dynamics of normal dithienylethene molecules either isolated or deposited on argon cluster

Aude Lietard, Giovanni Piani, Rodolphe Pollet, Benoit Soep, Jean-Michel Mestdagh, Lionel Poisson

Excited state dynamics of normal dithienylethene molecules either isolated or deposited on argon cluster†

Aude Lietard,[a,b] Giovanni Piani,[a] Rodolphe Pollet,[c] Benoît Soep[a,d], Jean-Michel Mestdagh[a], and Lionel Poisson*[a,d]

Real-time dynamics of the electronically excited open-ring isomer of 1,2-bis(2-methylbenzo[b]thiophen-3-yl)perfluorocyclopentene (BTF6) and 1,2-bis(2,4-dimethyl-5-phenyl-3-thienyl)perfluorocyclopentene (PTF6) molecules was investigated using a set-up that associates a molecular beam, femtosecond lasers and velocity map imaging. The molecules were either free in the gas phase or bound to an argon cluster. DFT and TDDFT calculations were performed on BTF6. The calculated vertical excitation energies indicate an excitation by the pump laser towards a superposition of S_5 and S_6 states. The free molecule dynamics was found to follow a three wavepacket model. One describes the parallel conformer (P) of these molecules. It is unreactive with respect to the ring closure reaction which is responsible for the photochromic property of these molecules. It has no observable decay at the experiment time scale (up to 350 ps). The other two wavepackets describe the reactive antiparallel conformer (AP). They are formed by an early splitting of the wavepacket that was launched initially by the pump laser. They can be considered as generated by excitation of different, essentially uncoupled, deformation modes. They subsequently evolve along independent pathways. One is directed ballistically towards a conical intersection (CI) and decays through the CI to a potential energy surface where it can no longer be detected. The other fraction of the wavepacket decays also towards undetected states but in this case the driving mechanism is a non-adiabatic electronic relaxation within a potential well of the energy surfaces where it was launched. When BTF6 and PTF6 molecules are bound to an argon cluster, the same three wavepacket model applies. The vibronic relaxation timespan is enhanced by a factor 5 and a larger fraction of AP conformers follows this pathway. In contrast, the time constant associated with the ballistic movement is enhanced by only a factor 2.

1 Introduction

Substituted dithienylethene molecules are known for their photochromic properties[1]. They have two stable isomers which can be interchanged with each other through a photoinduced reversible electrocyclic reaction. Besides, these isomers have quite different absorption regions and different conformations, this can be the source of many applications. Two representative examples are shown in Fig.1: 1,2-bis(2-methylbenzo[b]thiophen-3-yl)perfluorocyclopentene (BTF6 - $C_{23}H_{14}F_6S_2$) and 1,2-bis(2,4-dimethyl-5-phenyl-3-thienyl)perfluorocyclopentene (PTF6 - $C_{29}H_{22}F_6S_2$). In these molecules, the photochromic property is carried by the central six electron system. Its hexatriene (open-ring isomer) and 1,3-cyclohexadiene (closed-ring isomer) forms are commuted by a photocyclization/photoreversion reaction (called hereafter the ring-closure reaction). The open-ring isomer of dithienylethene molecules is called "*normal*" or "*inverse*" whether the S-atoms are bound to β or α C-atoms with respect to the C=C double bond of the perfluorocyclopentene ring. BTF6 and PTF6 molecules shown in Fig.1 are of the "*normal*" type.

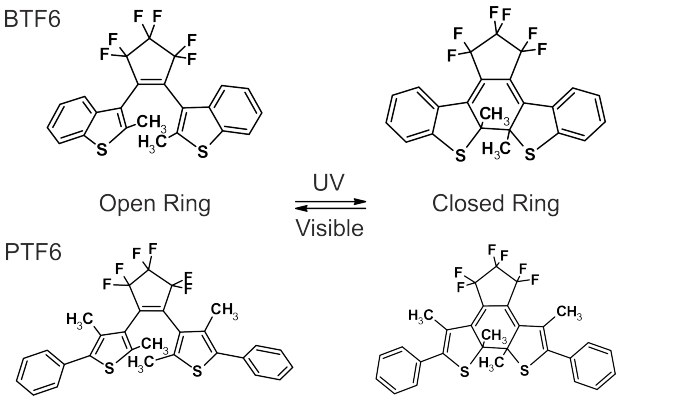

Fig. 1 Scheme of the photochromic reaction in BTF6 (1,2-bis(2-methylbenzo[b]thiophen-3-yl)perfluorocyclopentene; $C_{23}H_{14}F_6S_2$) and PTF6 (1,2-bis(2,4-dimethyl-5-phenyl-3-thienyl)perfluorocyclopentene; $C_{29}H_{22}F_6S_2$)

Many experiments, often complemented by TDDFT calculations, were conducted using femtosecond transient absorption spectroscopy technique to study the mechanism of the ring-closure and photoreversion reactions of dithienylethene molecules dissolved in solvents[2–5]. A concern exists indeed

† Electronic Supplementary Information (ESI) available: Additional figures.

[a]*Université Paris-Saclay, CEA, CNRS, LIDYL, 91191, Gif-sur-Yvette, France. E-mail: lionel.poisson@universite-paris-saclay.fr*

[b]*Present address: Department of Chemistry, Durham University, Durham DH1 3LE, United Kingdom*

[c]*Université Paris-Saclay, CEA, CNRS, NIMBE, 91191, Gif-sur-Yvette, France.*

[d]*Université Paris-Saclay, CNRS, Institut des Sciences Moléculaires d'Orsay, 91405, Orsay, France*

about the ring-closure reaction, the open-ring isomer has several conformers which are in thermal equilibrium at room temperature. They fall in two categories whether the aromatic groups of the side chains are parallel (P) or antiparallel (AP) to each other. P (resp. AP) isomers have a local C_s (resp. C_2) symmetry near the symmetry axis of the perfluorocycloepentene ring. Only AP isomers can undergo the ring closure reaction. Recently, Sotome et al.[3] showed that 1,2-bis(3-methyl-5-phenyl-2-thienyl)perfluorocyclopentene (an *"inverse"* dithienylethene molecule) has one P and two AP conformers, but only one of former makes the ring-closure reaction. Jarota et al.[2], Li et al.[4] and Hamdi et al.[5] investigated various *"normal"* dithienylethene molecules dissolved in solvents. They documented in particular which vibrational modes and non adiabatic processes (*e.g.* internal conversion) participate to the photocyclization reaction.

Solvents, even a non-polar ones like alkanes, certainly play an active role in the reaction process that is difficult to disentangle in the complex dynamics revealed by the works quoted above. It is therefore interesting to explore the intrinsic dynamics of dithienylethene molecules, *i.e.* the dynamics of these molecules when they are completely isolated in the gas phase. Time-resolved ultrafast ionization spectroscopy experiments were conducted for this purpose in a former work of the present author group. The intrinsic dynamics of a series of *"inverse"* dithienylethene molecules was studied in an experimental setup which associates a molecular beam, femtosecond lasers and a Velocity-Map-Imaging (VMI) spectrometer. This work, hereafter referred as *Paper I*, revealed the existence of several relaxation pathways.[6] Ultimately, it would be informative to add solvent molecules in a controlled way, to understand in which extent and by which mechanism, solvent molecules contribute/stimulate/control photochromic properties of these molecules. This has not been done, yet.

The present work is building up on *Paper I* using the same experimental setup. It includes, also state-of-the-art calculations. The excited state dynamics of BTF6 and PTF6, *"normal"* dithienylethene molecules shown in Fig.1, is investigated under two very different conditions: either these molecules are fully isolated in the gas phase or they are isolated within an argon cluster. In the former case, the intrinsic dynamics of the molecule is studied since the molecule cannot interact with an environment. In the latter case, isolation is achieved because a single molecule is carried by the argon clusters. However, the probed dynamics is not intrinsic, it includes mechanical and electronic perturbations due to the argon environment. Comparing the two regimes will show how a weakly invasive environment (argon cluster) may affect the intrinsic dynamics of the hosted molecule, a step towards understanding how a solvent affects the photochromic properties of dissolved species.

2 Experimental section

The experimental setup used in the present work is essentially the same as described in *Paper I* and in many of our former publications where isolated molecules (Refs. 6–10) or deposited one on argon clusters (Refs. 11–13) were studied. It associates a molecular beam, femtosecond lasers and a VMI. It is schemed in Fig. 3 of *Paper I*. Only features that are specific to the present work are described below.

BTF6 and PTF6 molecules were purchased as solid powder from TCI Europe under the references B2287 and B2629, respectively. No further purification was achieved.

Beam isolated molecules - For their use as vapor in the beam isolation experiment, BTF6 (or PTF6) powder was mixed with graphite, then the mixture was pressed into a tablet at 15 bar. The sample tablet was put in a oven mounted directly on the nozzle plate of a pulsed valve (nozzle diameter 0.5 mm) maintained at a temperature of $\sim$ 370 K ($\sim$ 380 K for PTF6). The carrier gas was helium (2 bar stagnation pressure). The gas expansion was collimated by a 1 mm diameter skimmer set at a 30 mm distance from the oven orifice (1.5 mm diameter)[10].

Molecules deposited on Ar clusters - The above beam setup was modified as follows. The helium carrier gas was replaced by argon (15 bar stagnation pressure), the nozzle was changed (0.1 mm diameter), and a pick-up region was added. Under this configuration, a log-normal distribution of argon clusters was generated with an average size of $\approx$500 argon atoms.[13,14] Then, the cluster beam passed over a crucible containing the BTF6 (or PTF6) powder maintained at $\sim$ 340 K ($\sim$ 350 K for PTF6). These temperatures were chosen to operate slightly above the apparition threshold of the PE signal. Hence, the vapor pressure of BTF6 and PTF6 were large enough to ensure that a significant number of sticky collisions (pick-up) deposit a single molecule on the clusters, and low enough to make negligibly small the probability of picking-up two molecules on the same cluster. This procedure takes advantage of the Poisson statistics which governs the pick-up technique, a no-memory stochastic process between successive events (see Ref. 12). Hosted molecules are believed to be thermalized at the cluster temperature (32 ± 2 K)[15].

Interaction with femtosecond pump and probe lasers - After its generation, the molecular beam entered the interaction chamber where it crossed the pump and probe laser beams, generated from the LUCA femtosecond Ti:sapphire laser of the European facility SLIC Laserlab (http://iramis.cea.fr/slic/). The latter operated in the range 789-792 nm with a spectral width (FWHM) of 22 nm and a repetition rate of 20 Hz. Its third harmonic, measured between 265.1 and 266.3 nm, was generated by frequency doubling and wave mixing in BBO crystals. It was used as pump laser. The probe laser beam was taken from the remaining Ti:sapphire laser beam. It operated by ionization through a multiphoton scheme. A delay line (moving mirrors on a motorised translation stage) was used to vary the time delay τ between the pump and probe laser pulses. The FWHM cross-correlation time between the pump and probe laser pulses was measured to *ca* 80 fs. Note that the multiphoton detection did not provide enough energy to ionize ground state products. In particular, no information is given whether the closed ring or the opened ring isomer of the molecule under study is formed as final product. Only timespans of electronically excited states are documented.

The synthesis of BTF6 and PTF6 molecules forms the open-ring isomer almost exclusively.[16] The corresponding absorption spec-

tra have been recorded in *n*-hexane.[16–18] They exhibit a strong absorption band which matches the wavelength of the pump laser (265.1-266.3 nm). The results below thus concern the photoinduced dynamics of the open-ring isomer, exclusively.

Detection - Charged particles generated by the probe laser ionization were detected using a time-of-flight mass spectrometer (TOF-MS) for the photoions (PI) and a VMI for the photoelectrons (PE). The 20 Hz recurrence of the laser precluded coincidence experiments to be performed. The number of events produced per second under coincidence conditions is indeed very low ($\sim 1s^{-1}$) and would lead to an unrealistically long acquisition time given more than $\sim 10^4$ events are required for imaging experiments. Hence, PI and PE were recorded separately. Coupled with the fs-laser, the VMI detection allowed us performing femtosecond time resolved PE spectroscopy (fs-TRPES) experiments.[19,20]

Treatment of the fs-TRPES data - To get the full information from fs-TRPES measurements, 3D radial and angular distributions of PE's were reconstructed from the raw 2D images provided by the VMI detector. Advantage was taken that the two 3D distributions have a cylindrical symmetry along the polarization direction of the probe laser, which was parallel to the plane of the VMI. The full reconstruction was performed using the pBASEX algorithm based on the inverse Abel transform.[21] Raw images suggested an isotropic distribution of PE's and the inversion procedure was limited to an isotropic decomposition. PE energies were calibrated as in Refs. 8,12, using the multiphoton ionization of molecular oxygen as reference. In contrast to a recent work of our group,[22] no rotational anisotropy was observed here. Hence, the relative direction of polarization of the pump and probe lasers (parallel or perpendicular) were not controlled and no treatment such as in Ref. 23 was performed.

The information provided by the pBASEX analysis of the fs-TRPES data was a series of PE spectra. Each one corresponded to a different τ value.

3 Computational strategy

Present computations aimed at calculating vertical excitation energies and optimize excited-state geometries of isolated BTF6 molecule. Density Functional Theory (DFT) and Time-Dependent Density Functional Theory (TDDFT) calculations were performed using the Turbomole program suite.[24] The molecule initial geometry was adapted from X-ray data.[25]

The basis sets choice was guided by checking the convergence of structural parameters (distances, angles) as the size of the basis set increased (from split valence to triple zeta valence quality). Basis sets of triple zeta valence quality complemented by small sets of polarization functions (def2-TZVP) were chosen.

The B3LYP hybrid functional was preferred to gradient-corrected approximations (GGA), such as PBE, for conducting the TDDFT calculations. This avoids the contamination of the calculated absorption spectrum by spurious charge-transfer excitations as demonstrated by Pollet and Brenner, taking two amino acids as examples.[26] Informatively, a recent study has shown that absorption wavelengths predicted by the B3LYP density functional for both open and closed isomers of perfluorocyclopentene derivatives agree within 10 nm with the slightly more accurate M05 hybrid meta GGA functional.[27]

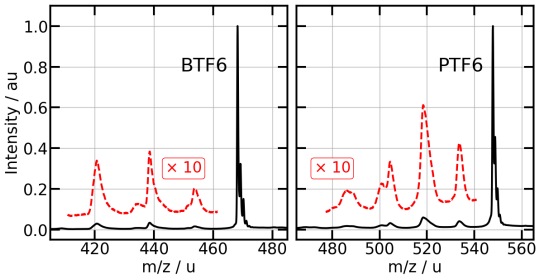

Fig. 2 Mass spectra of BTF6 and PTF6 molecules. The red dashed curves magnify the fragment intensities by a factor 10.

To estimate the amount of dispersion effects and to control their influence for the molecule under study, a semi-local functional including atom-pairwise C_6/R^6 and C_8/R^8 corrections (*i.e.*, B97-D3) was also used.[28]

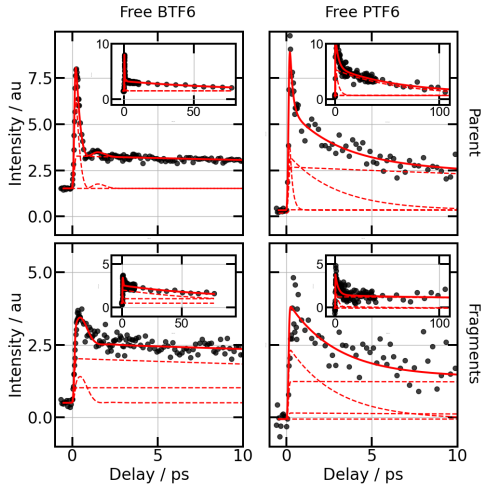

Fig. 3 PI signal as a function of the time delay between the pump (265 nm) and probe (795 nm) laser pulses. Insets show the evolution up to 80 ps in left panels for free BTF6 (up to 100 ps in right panels for free PTF6). Top panels show the evolution of the parent PI signal and bottom panels that of the PI fragments (all summed together). Black dots are experimental data and full red curves, their fit using functions defined in Tab.1. Red dashed curves are contributions to the fit.

4 Experimental results

4.1 PI's in free BTF6 and free PTF6 experiments

Mass spectra - Mass spectra could be collected only in free BTF6 and free PTF6 experiments. When probing BTF6 and PTF6 molecules that are bound to an argon cluster, the resulting PI have indeed a too large mass/charge ratio (m/z) to be detected using the TOF-MS, as we do not furnish enough energy to ionize and desorb the ion from the cluster. Fig.2 sums mass spectra recorded at a function of τ. Intense narrow peaks are observed at m/z = 468 u and 548 u. They are assigned to the parent mass of BTF6 and PTF6 (molecular weights, 486.47 g mol^{-1} and 548.61g mol^{-1}, respectively). The assignment is consistent with

Table 1 Time constants τ_i (in ps) of exponential decay functions used to fit the PI and PE time evolution signals in Figs.3 and 5. Weight$_i$ gives the relative weight of the exponential function of time constant τ_i when fitting PE signals (weight$_1$+weight$_2$+weight$_3 \approx 100$). NM: non measurable.

		BTF6	PTF6	BTF6(Ar)$_n$	PTF6(Ar)$_n$
	(PI)	0.425 ± 0.04	NM	–	–
τ_1	(PE)	0.54 ± 0.1	1.2 ± 0.2	1 ± 0.5	2.4 ± 0.3
	weight$_1$	44.7±4	39.7±2	9.9±3	43.2±4
	(PI)	75 ± 5	3.2 ± 1	–	–
τ_2	(PE)	80 ± 10	11.4 ± 2	400±50	57 ± 5
	weight$_2$	31.7±3	37.6±2	82.2±7	49.8±4
	(PI)	Plateau	Plateau	–	–
τ_3	(PE)	Plateau	Plateau	Plateau	Plateau
	weight$_3$	23.6±2	22.6±0.5	8±8	7.9±1

the fine structure of the peaks as it matches the one expected from the isotopic distribution of C and S atoms contained in the molecules.

Low intensity peaks are also observed in Fig.2. A closer look on them shows a much larger width than observed on the parent peaks. Broad peaks in a TOF-MS indicate that the corresponding ions carry an isotropically distributed recoil velocity. This happen when then ions have been produced by a fragmentation process. As a consequence, they cannot be assigned to parent peaks of impurities of small mass in the beam. Instead, they result of the parent PI fragmentation following a $n \geq 3$ multiphoton ionization by the probe laser, i.e. after ≥ 4.6 eV energy was deposited by the probe laser. According to their m/z ratio, they correspond to the loss of a CH_3 group and/or a S atom in a complex rearrangement of the PI after the multiphoton ionization process.

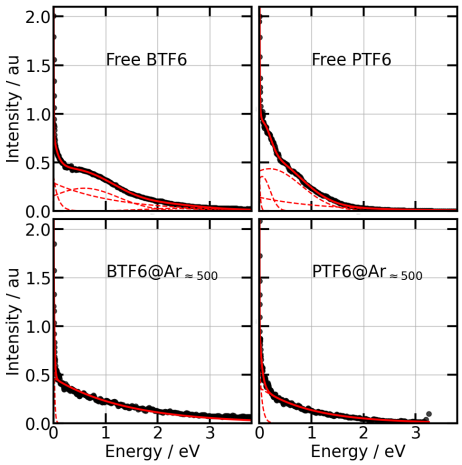

Fig. 4 PE spectra in free BTF6, free PTF6, BTF6(Ar)$_{\approx 500}$ and PTF6(Ar)$_{\approx 500}$ experiments. Black dots are experimental data and full red curves, their respective fit, using the functions defined in Tab.2. Red dashed curves are each fit components.

Fig.3 reports the parent PI peak intensity (top panels) and the summed intensities of the fragment PI peaks (bottom panels) as a function of τ in free BTF6 (left panels) and free PTF6 (right panels) experiments. Multi-exponential decays are observed. Their shape differs from one panel to the other. A rapid component is prominently observed on BTF6 parent PI's (top left panel). This component may exist in the corresponding PTF6 signal (top right panel), nevertheless it is close to the experimental noise. The rapid component is considerably reduced when fragment PI peaks are considered. An oscillation of small amplitude appears during the first 3 ps evolution of the parent PI peak in the BTF6 experiment.

The same strategy as in *Paper I* was applied to extract characteristic time constants from the experimental data of Fig.3. BTF6 and PTF6 data were fitted with a linear combination of three exponential decay functions after each function was convoluted by a Gaussian function (FWHM 80 fs) representing the instrument response. The same set of constant was used to fit the parent and fragment PI's. Only their relative intensity was changed. Best fit constants are listed in Tab.1. Note that in PTF6 experiment, the rapid component is not documented since it has a too small intensity compared to the experimental noise.

4.2 Photoelectrons

4.2.1 Free BTF6 and PTF6 molecules

Series of PE images were recorded as a function of τ in both BTF6 and PTF6 experiments. As explained in Sec.2, the treatment of each image by the pBASEX algorithm provided us a series of PE spectra as a function of τ. They are all summed together in Fig.4 (top panels) where they are adequately fitted (red curves) as the sum of three exponential functions $\exp(-\frac{E}{E_i})$ (with E is the PE energy) and two Gaussian functions $\exp(-\frac{(E-\mu_i)^2}{2\sigma_i^2})$ using all parameters listed in Tab.2. The fit functions were arbitrary determined, provided they are adequate for properly fitting the entire set of PE-spectra that were recorded. The idea with these functions was to know if certain classes of PE had a peculiar dependence with the pump/probe time delay. Actually, they do. The corresponding data are now included in the ESI†(Fig. S1). Unfortunately, without a full theoretical description in the spirit as the "field-induced surface hopping simulations" reported in Ref. 29, it is difficult, if not impossible, to get convincing information from these data. Hence, only the total PE signal is considered here, *i.e.* the sum of the five fit contributions is shown in Fig.5 (BTF6, black dots; PTF6, red dots) as a function of τ. The full investigation over τ is shown in the top panel of the figure, and a closer look over the first 10 ps in the bottom panel. As for PI's in Fig.3, a multiexponential decay is observed and small amplitude oscillations are superimposed in BTF6 case. In the same spirit as for PI data, BTF6 and PTF6 PE data were fitted with a linear combination of three exponential decay functions after proper convolution by the instrument response. Best fit parameters are listed in Tab. 1.

4.2.2 BTF6 and PTF6 bound to argon clusters

BTF6(Ar)$_{\approx 500}$ and PTF6(Ar)$_{\approx 500}$ experiments were conducted in the same way as the experiments reported above for the free molecules. The same data treatment was also applied. The corresponding results are shown in bottom panels of Fig.4 and fitted using functions defined in Tab. 2. Unlike spectra recorded in free BTF6 and free PTF6 experiments (top panels), only exponential

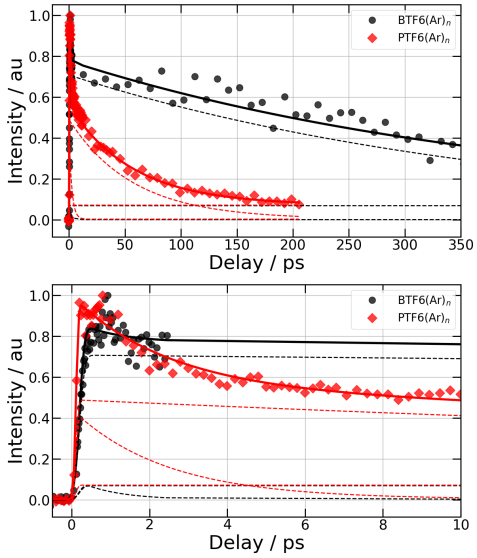

Fig. 6 Same caption as Fig.5 for BTF6(Ar)$_{\approx 500}$ and PTF6(Ar)$_{\approx 500}$ experiments.

Table 2 Parameters of the exponential and Gaussian functions used to fit the PE spectra in Fig.4.

Fit functions		BTF6	PTF6	BTF6(Ar)$_n$	PTF6(Ar)$_n$
$\exp(-\frac{E}{E_i})$	E_1	0.004	0.004	0.002	0.002
	E_2	0.090	0.02	0.015	0.050
	E_3	1.200	1.20	1.400	1.000
$\exp(-\frac{(E-\mu_i)^2}{2\sigma_i^2})$	μ_1	0.59	0.05		
	σ_1	0.65	0.15		
	μ_2	2.27	0.20		
	σ_2	0.57	0.60		

functions were needed for an adequate fit. The τ dependence of the total PE signals recorded in TF6(Ar)$_{\approx 500}$ (black dots) and PTF6(Ar)$_{\approx 500}$ (red dots) experiments are reported in Fig.6.

5 Computational results

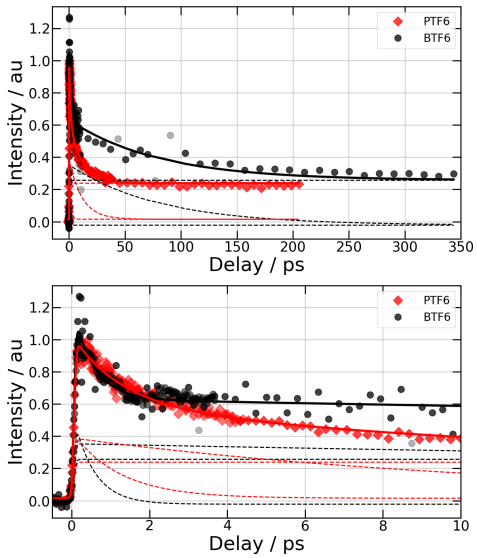

Fig. 5 Total PE signal in free BTF6 (black dots) and free PTF6 (red diamonds) experiments as a function of τ, the time delay between the pump (265 nm) and probe (795 nm) laser pulses. The top panel show the evolution up to several hundreds of picoseconds. The bottom panel

Computations were carried out on the open-ring isomer of BTF6. As expected, the ground state of the C_2 (or AP) and C_s (P) conformers were found nearly isoenergetic, the former being slightly more stable. Relative energies obtained with PBE, B3LYP, and B97-D3 density functionals are 2.45, 2.34, and 0.99 kJ.mol^{-1}, respectively. These values have to be compared with the B3LYP value of 1.51 kJ.mol^{-1} reported by Asano et al. with the poorer basis set 6-31G.[30]

Absolute energies of the C_2 (AP) and C_s (P) conformers were significantly corrected when dispersion effects were included (see Sec.3). This lowered also their relative energy, the overstability of the AP conformer being preserved. Informatively, optimized geometries were not very sensitive to the choice of the density functional. Minimized root mean square deviations are indeed less than 0.24 Å for AP conformer and 0.27 Å for P conformer.

Calculated distances between the two reactive carbon atoms are reported in Tab.3. Whatever the conformer and the calculation level, they are slightly smaller than the value of 4.2 Å that Kobatake et al. have proposed as a criterion to predict the feasibility of the ring closure reaction in the monocrystalline phase.[31]

Table 3 Distance (in Å) between the two reactive carbon atoms for the C_2 (AP) and C_s (P) conformers from different density functionals, using the def2-TZVP basis set.

Conformer	PBE	B3LYP	B97-D3
C_2 (AP)	3.93	4.16	3.69
C_s (P)	4.14	4.16	4.02

Vertical excitation energies of the photoreactive AP (C_2 symmetry) conformer of BTF6 were provided by the TDDFT calculations (B3LYP hybrid functional). The ten lowest energies are listed in Tab.4 together with the corresponding main transition between molecular orbitals. Several of these orbitals are shown in Fig.7. All transitions leading to the LUMO have a strong charge transfer character, due to a strong transfer of the electron density from the benzothiophenyl subunits to the perfluorocyclopentene one. As mentioned before, the stability of such excitation is often overestimated within TDDFT[26].

Regarding the present experiment, the most promising transitions are those to states S_5 and S_6. The corresponding $S_0 \rightarrow S_x$ excitation is mainly local, with a strong $\pi \rightarrow \pi^*$ character centered on the C=C double bonds of the benzothiophène groups, which are facing each other. Associated electric dipole transition moments are large (1.21 and 1.59 Debye for S_5 and S_6, respectively) and absorption wavelengths (279 and 271 nm read in Tab.4) are close to the wavelength of the pump laser (265.1-266.3 nm). Geometries of S_5 and S_6 states have tentatively been optimized

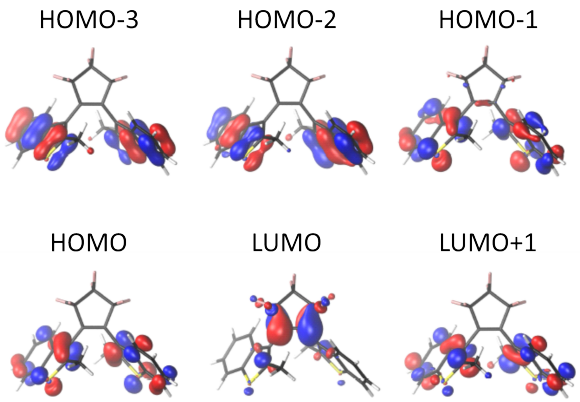

Fig. 7 Several molecular orbitals of BTF6 molecule (C_2 (AP) conformer), calculated at the B3LYP/def2-TZVP level.

with TDDFT. The task was actually extremely difficult given the multiconfigurational character of these states. It could only be achieved for S_5. Doing so, the distance between the two reactive carbon atoms has slightly decreased from 4.16 Å to 4.04 Å, not enough to achieve a ring closure. This suggests that no "easy-to-find" barrierless pathway exists within this surface towards photocyclization. This agrees with a CIS/6-31G calculation reporting that the two C atoms do not come closer than 3.65 Å.[30]

Table 4 Vertical excitation energies of the ground state BTF6 C_2 (AP) conformer from TDDFT(B3LYP/def2-TZVP) calculations.

Final state	λ (nm)	Oscillator strength	Main transition	Weight (%)
S_1	344	0.049	HOMO → LUMO	98
S_2	325	0.016	HOMO-1 → LUMO	96
S_3	295	0.005	HOMO-2 → LUMO	97
S_4	293	0.002	HOMO-3 → LUMO	93
S_5	279	0.024	HOMO → LUMO+1	88
S_6	271	0.044	HOMO-1 → LUMO+1	62
S_7	270	0.018	HOMO → LUMO+2	78
S_8	266	0.008	HOMO-1 → LUMO+2	33
S_9	258	0.059	HOMO → LUMO+4	29
S_10	257	0.009	HOMO-1 → LUMO+2	57

6 Discussion

6.1 Dynamics of free BTF6 and free PTF6 molecules

Two independent conformers AP and P are present - We mentioned several times already that open-ring isomers of BTF6 and PTF6 molecules have two conformers labeled AP (of C_2 symmetry) and P (C_s) whether the aromatic sidebands are antiparallel (AP) or parallel (P). Uchida et al. reported a room temperature NMR study of BTF6 where two distinct peaks appear in the ratio 65:35. They were assigned to AP and P conformers, respectively.[32] The same kind of observation was done for PTF6 with an abundance ratio of 48:52.[33]. The two peaks in the NMR studies at room temperature suggest that a slow Boltzmann equilibrium is at play. For BTF6, the 65:35 ratio suggests an over-stability by 1.05 kJ.mol^{-1} for the AP conformer, a value which falls in the range predicted by calculations reported in Sec.5 (0.99-2.45 kJ.mol^{-1}). A quantitative agreement is found with the 0.99 kJ.mol^{-1} value obtained with the B97-D3 density functional. The ratio 48:52 found in NMR study on PTF6 suggests an almost thermo-neutral equilibrium between the two conformers of this molecule.

In line with NMR studies recalled above and also with present calculations, which predict the stability of BTF6 AP and P conformers. We consider that both are present in BTF6 and PTF6 vapors used here to generate the molecular beams of the present study, either free or bound to argon clusters.

Calculated excitation energies reported in Tab. 4 for BTF6 indicate that, within a pump laser wavelength in the range 265.1-266.3 nm, the AP conformer states S_5 and S_6 can be excited through strong $\pi \rightarrow \pi^*$ transitions. Although the electronic states of the P conformer were not calculated here, we consider that AP and P conformers have likely a very similar electronic configuration, thus strongly allowed transitions are also expected in the same range of wavelengths. A work of Hamdi et al. confirms this expectation for PTF6 in a chloroform (trichloromethane) solution.[5] They measured and calculated (PCM-TDDFT/CAM-B3LYP/6-311+G(2d,p)) indeed maximum absorbance wavelengths at 266 and 267 nm for AP and P conformers.

Two points have emerged from the discussion above: *i)* P and AP conformers are both present in all experiments performed here (free BTF6, free PTF6, BTF6(Ar)$_{\approx 500}$ and PTF6(Ar)$_{\approx 500}$); *ii)* the pump laser pulse excites both of them to high lying states (S_5 and/or S_6) with about the same excess vibrational energy. Given the unstructured spectra observed in Fig.4, the ionization of these species by the probe laser leads to strongly overlapping PE bands, where AP and P contributions cannot be disentangled. It might be though that, given the excess energy provided by the electronic excitation, the equilibrium between the P and AP isomers could be rapid when excited. The numerous works recalled above show that in solved, this it is not the case.

Conformer AP: a dynamics along two independent pathways - It is known for a long time that, in solution, the ring-closure reaction of electronically excited dithienylethene derivatives, which BTF6 and PTF6 belong to, follows two pathways of different nature: a fast process occurring in the pico- or subpicosecond regime and a slow one occurring in several hundred of picoseconds, which is sensitive to the solvent viscosity.[16,34]

This was interpreted theoretically by Boggio-Pasqua et al.[35] who mapped S_0 and S_1 potential energy surfaces of several diarylethene and dithienylethene molecules and run dynamical calculations on these surfaces. One of these molecules, 1,2-bis(2-methyl-5-phenyl-3-thienyl)perfluorocyclopentene, is very close to PTF6 (only the two methyl groups are missing). According to these calculations, the photochromic character stems from a conical intersection (CI) at an intermediate geometry between those of the open and closed ring isomers. The calculated structure shows, as first peculiarity, that the reaction pathway connecting the open and closed-ring isomers is not contained in the space that defines the CI which promotes the ring closure reaction. Hence, an intrinsically multidimensional dynamics is at play to

access the CI. As second peculiarity, the calculated CI is energetically above the well of the S_1 potential energy surface (see scheme 2 of Ref. 35). Hence, we conclude from these results that the trajectories which do not cross the CI can stay within the S_1 minimum for a long time after the excess energy is evacuated along perpendicular degrees of freedom. A more recent theoretical work of Perrier et al. partly confirms this picture, in particular the presence of the CI away from the well of S_1 potential energy surface.[36]

An even more recent experimental and theoretical work by Hamdi et al.[5] paints a somewhat more complicated picture of the excited state dynamics of PTF6 P/AP conformers in chloroform following excitation at 320 nm, in which triplet states are involved. These authors showed that the non-photochromic conformer P undergoes the following sequential relaxation after photoexcitation $\xrightarrow{200fs}$ S_1 $\xrightarrow{55ps}$ ^{3}P $\xrightarrow{2.5ms}$, whereas the AP conformer evolves along two parallel pathways from the Franck-Condon region. One promotes the photocyclization reaction in 100 fs through a CI, while the second is a relaxation within the electronically excited surface followed by an intersystem crossing process towards a triplet state in 1 ps.

In the present work, whatever the performed experiments (fully isolated molecules or molecules weakly bound to argon clusters), the initial electronic excitation of BTF6 and PTF6 molecules is larger than in the works of Refs. 5,35,36. High lying states (S_5 and/or S_6) were populated here by the pump laser, whereas excitation to the S_1 potential energy surface was performed in Refs. 35 and 5 (S_1 and S_2 in Ref. 36). The present initial excitation is believed to be transferred very rapidly, within (much) less than 100 fs to the S_2 or S_1 surfaces through a series of conical intersections. Such rapid evolution toward low lying excited states have been observed easily in former works of the present group of authors (e.g. Refs. 29,37,38). In contrast, here, the energy resolved PE signals shown in Fig. S1 of the ESI†do not exhibit features that can be assigned to this early dynamics. The region below 100 or 200 fs is very confused and the only reliable time evolutions that are apparent on this figure are the low one reported in Tab.1 that we assign to dynamics within the S_1 energy surface. The discussion that follows uses the picture brought by Refs. 5,35,36 as a guideline and shows that the present data are consistent with this picture. From the theoretical calculations of Ref. 35,36 and from the experiments of Ref. 5 conducted in solvents, we know that two parallel relaxation pathways are active simultaneously in the BTF6 AP conformer. A similar situation was met in the gas phase experiment on *"inverse"* dithienylethene molecules in *Paper I*. This is however not usual in gas phase femtochemistry where a single process commonly dominates each step in the evolution of electronically excited species. Sequential dynamics is then observed and the wavepacket, which has been launched in the Franck-Condon region of an excited potential energy surface by the pump laser, spreads and does not split significantly into sub-wavepackets, even when it transfers to lower energy surfaces. The picture in *Paper I* and Ref. 5 and that followed in the present work is very different. As usual in gas phase femtochemistry, the pump laser launches a vibrational wavepacket in a region of potential energy surfaces where several deformation modes of the molecule are activated. The wavepacket subsequently spreads over the initial potential energy surfaces and, in the present work, transfers very rapidly (see above) to the S_1 surface. The difference here with ordinary situations in gas phase femtochemistry is suggested by the theoretical work of Boggio-Pasqua et al. that has been recalled above.[35] The CI, which gives access to the ring closure reaction, is energetically above the well of the S_1 surface and found along coordinates that do not include the reaction path of the ring closure reaction. As a result of the energetic constraints the WP gives only partial access to the CI. Instead, part of it reaches the CI and the remaining part redistributes the excess energy within the accessible deformation modes of the molecule before transferring to the ground state.

Conformer AP: the final photoreaction product - The paragraph above showed that the excited state dynamics of the AP conformer of BTF6 and PTF6 proceeds along two independent channels. One may wonder if both are leading to the same final product or to two different products. Unfortunately, neither present PI or PE signals carry information that informs on final products. They are formed in the ground state and cannot be ionized by the probe laser. Clues to answer this question are provided by experiments performed in the condensed phase where the quantum yield of the photocyclization was measured. For BTF6 in hexane, the quantum yield was measured as 36% after excitation at 258 nm, whereas the reactive AP conformer was present at only 65%.[32] Hence, approximately one half only of the photoexcited AP conformers makes a ring-closure reaction. This suggests that the two parts of the initial wavepacket in BTF6 AP conformer do not lead to the same final product. With PTF6, the situation is confusing. The photocyclization quantum yield was measured to 0.46,[39] whereas the population of the P conformer was 48%.[33] This would suggest that 100% of the laser excited AP conformer of PTF6 go to photocyclization, whatever the channel that is followed. This conflicts however with the work of Hamdi et al., which shows that only a part of the initial wavepacket goes to the closed ring isomer, whereas the other goes to the open ring isomer. The issue on the final photoproduct is complemented below when comparing present data on BTF6(Ar)$_{\approx 500}$ and PTF6(Ar)$_{\approx 500}$ experiments with data of the literature on BTF6 and PTF6 monocrystals.

Assignment of the measured time constants according to a three wavepacket model - The paragraphs above suggest that three wavepackets (WP_1, WP_2 and WP_3) are to be detected in the present experiment. They are schemed in Fig.8. WP_1 and WP_2 are sub-wavepackets of the initial wavepacket WP_0 on the AP conformer, which has split in two parts after transferring to the S_1 potential energy surface through unresolved non-radiative processes. WP_1 reaches the CI whereas WP_2, the remaining part of the initial wavepacket, stays within the well of the S_1 potential energy surface. WP_1 and WP_2 evolve on regions of the S_1 potential energy surface which have a very different shape. WP_1 experiences uphill slopes to reach the CI that are not experienced by WP_2. Likely, WP_1 and WP_2 loose the relative coherence (loss of intrication) they had in WP_0 immediately after the pump pulse. They are considered therefore as documenting two independent

reaction pathways.

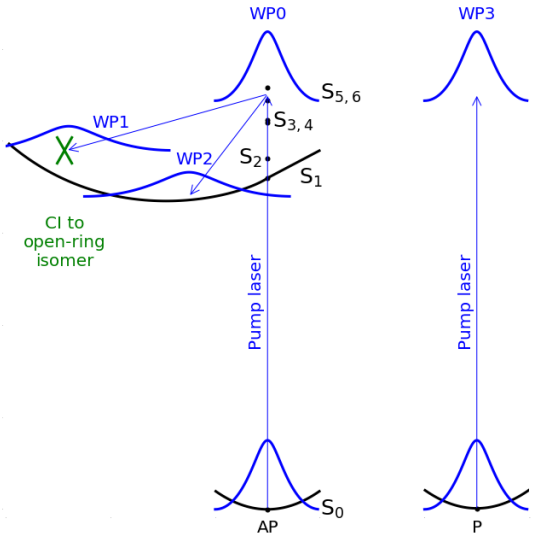

Fig. 8 Scheme showing the three wavepackets WP_0, WP_1, WP_2 and WP_3 used to discuss the dynamics of electronically excited BTF6 and PTF6. The dots showing the S_0-S_6 states of the AP conformer are located according to the vertical excitation energies given in Tab.4 for BTF6. The abscissa schemes the C-C bond formation coordinate. The other indications, like potential curves, CI and wavepackets were drawn to be consistent with the current discussion.

In this model, WP_3 describes the unreactive P conformer, which is of course fully independent from WP_1 and WP_2. It is not expected to exhibit an ultrafast dynamics upon excitation. Instead, the lifetime of the electronically excited state of P that is populated by the pump laser certainly exceeds the timescale of the present experiment. The exponential function of time constant τ_3, which appears as a plateau in Tab.1, is thus assigned to detection of WP_3. Still considering evolution timescales within the three wavepacket model, WP_1, which experiences an uphill CI, likely goes very rapidly out of detection and must be associated with a very small time constant. τ_1 is therefore assigned to the detection of WP_1. Consequently, τ_2 and WP_2 must be associated. The present assignment matches that in *Paper I* for the I-DTE molecule ($C_{17}H_{14}F_6S_2$, bis(3,5-dimethyl-2-thienyl)-perfluorocyclopentene). The discussion in *Paper I* can thus be followed, in particular that relating τ_1 and τ_2, the decay time constants of WP_1 and WP_2 and the excitation of two distinct categories of vibrational modes. The modes that target the CI are at the origin of WP_1 and can be described as driving a ballistic movement. Accordingly, τ_1 represents also the access time to the CI for the fraction of the initial wavepacket that is directed in the proper direction. In contrast, WP_2 and τ_2 are associated with the other deformation modes of the molecule and describe electronic deexcitation towards lower energy states through vibronic couplings within the thermal bath formed by the electronic and vibrational degrees of freedom of the molecule. τ_2 thus appears, in this model, as the characteristic time of vibronic relaxation towards undetected lower electronic states (singlets or triplets) as discussed in *Paper I*.

It is interesting to notice in Tab. 1 that τ_2 is about a factor 10 smaller for PTF6 than for BTF6 (3.2-11.4 ps *versus* 75-80 ps). This can be put in relation with the larger number of degrees of freedom in PTF6 and therefore the larger density of state which likely enhances the efficiency of vibronic relaxation down to undetectable electronic states of this molecules. This observation is also consistent with the ratio $\frac{weight_1}{weight_2}$ which is smaller for PTF6 (1.06 *versus* 1.41 for BTF6): additional deformation modes in PTF6 are indeed likely orthogonal to modes that generate the ballistic movement of WP_1 towards the CI.

Oscillation regimes in BTF6 - Small amplitude oscillations are observed in BTF6 experiments, both in PI (Fig.3 top left panel, and in ESI†Fig. S2) and PE signals (Fig.5 bottom panel, and in ESI†Fig. S2). They are damped as the decay of time constant τ_2. It reveals two oscillation regimes with ≈620 fs (54 cm^{-1} energy) and ≈1.8 ps (18 cm^{-1}) periods. These oscillations are revealed by the multiphoton detection, because accidental resonance efficiencies are modulated by the molecular vibration.

The 54 cm^{-1} energy oscillation is strikingly close to the value of 55.31 cm^{-1} that Jean-Ruel et al. have calculated as the vibrational mode of lowest energy for the PTF6 open-ring conformer in its ground electronic state.[40] This mode, likely present in BTF6 too, is associated with a torsional motion of the two pendant side groups and affects the C···C gap that drives the ring closure reaction. Care must be taken however with this analogy: first, because it stems from calculations on the ground electronic state, whereas the closure reaction proceed on excited surfaces and of course because the calculation was performed on PTF6, where no oscillation was observed, and not on BTF6 where oscillations are presently discussed.

Given the aforementioned calculations of Jean-Ruel et al. we do not expect that BTF6, which is a smaller molecule than PTF6, has a vibrational mode of lower energy than 55.31 cm^{-1}, which has been mentioned above as the mode of lowest energy in PTF6. The 18 cm^{-1} oscillation is more likely associated with a quantum beat between two vibrational modes that are coherently excited, either directly during the pump laser excitation, or indirectly during the initial stage of the wavepacket movement as it was previously described for the DABCO molecule.[41] Interestingly, low energy modes calculated by Jean-Ruel et al. at 308.62 and 322.95 cm^{-1} for of PTF6 differ by 14.33 cm^{-1}. Equivalent modes in BTF6 may account for the 18 cm^{-1} observed here.

6.2 Dynamics of BTF6 and PTF6 molecules bound to an argon cluster

Tab. 1 compares time constants τ_i and weights $weight_i$ of wavepackets WP_1, WP_2 and WP_3 whether BTF6 and PTF6 molecules are free (second and third columns) or bound to an argon cluster (last two columns). In view of the most complete PE data, the WP_1 weight ($weight_1$) is severely reduced for BTF6 in the argon environment, whereas τ_1 is enhanced by a factor 2 for both BTF6 and PTF6 molecules. The main effect for WP_2 is an increase of τ_2 by a factor five. Finally the WP_3 weight is notably reduced for both molecules in argon cluster experiments. These differences are discussed in the following.

The small weight of WP_3 in the cluster environment suggests that the population of conformer P, the least stable one, has decreased after BTF6 and PTF6 molecules did a sticky collision with the argon cluster. From the present calculation, the AP conformer is more stable than P by 1-2.5 kJ.mol^{-1}. Perrier et al. calculated an energy barrier of $\approx$ 11 kJ.mol^{-1} for the isomerization of the least stable conformer into the most stable one.[36] Such a barrier is large compared to the cluster temperature (32 K) and does not allow the P and AP conformer to exchange when the BTF6 and PTF6 molecules are thermalized at the cluster temperature. However, these molecules do a sticky collision with the cluster, $\approx$ 0.2 eV ($\approx$20 kJ.mol^{-1}) collision energy has to be relaxed towards the clusters. This energy is sufficient to induce isomerization between the AP and P conformers, hence lowering the population of the P conformer and therefore the weight of WP_3. The percentage of P conformer is therefore expected to be reduced when comparing the isolated to the deposited molecules. This is consistent with the values of weight$_3$ in Tab. 1 and, indirectly, confirms the assignment of WP_3 to the P conformer.

The presence of an argon cluster has a limited effect on τ_1, which increases by a factor $\approx$2. However, such effect of the argon atoms on the reaction dynamics can be understood with the following picture. Indeed, this time increase indicates that BTF6 and PTF6 deformation modes directing WP_1 ballistically towards the CI are poorly coupled to numerous degrees of freedom brought by an argon cluster. Nevertheless, several argon atoms may be carried into movement by the deformations that drive the wavepacket. This couples partly WP_1 with a thermal bath formed by the argon atoms and may account for the τ_1 increase. Nevertheless, the most dramatic effect of the argon environment is the ballistic wavepacket "colliding" one or several repulsive walls associated with argon atoms and deviates from reaching the CI. This picture is consistent with calculations of Boggio-Pasqua et al.[35] and Perrier et al.[36] who showed that the CI is located at a fairly high energy and difficult to access according to the deviation of its geometry compared to the initial and final ones. Hence, argon atoms may have an obstruction effect which redirects a substantial part of WP_1 into WP_2. Apparently, this effect is especially strong with BTF6 where the WP_1 weight falls down to 9.9% whereas the WP_2 one moves up to 82.2% in argon environment (see Tab. 1).

Within this picture, the argon cluster effect is significantly different when considering the vibronic relaxation within the potential well of the excited potential energy surface, *i.e.* when considering the quantities τ_2 and *weight*$_2$ characterizing WP_2. The main effect concerns τ_2, which increases by a factor five for both BTF6 and PTF6 (see Tab. 1). This is surprising at a first glance, since the argon cluster offers many additional degrees of freedom that should increase the efficiency of vibronic relaxation. This is not counting however with the cooling efficiency of an argon cluster with respect to the hosted molecule internal degrees of freedom. This cooling time scale was measured to several hundreds of picosecond in Ref. 13, not enough to compete efficiently with vibronic coupling within the molecule but enough to cool down the hosted molecule to the cluster temperature prior the dynamics is turned on by the pump laser. Hence, the excited state relaxation proceeds within an initially colder molecule, when the latter is bound to a cluster than when fully isolated. The internal energy of BTF6 and PTF6 molecules that stay trapped within the well of the excited potential energy surface is therefore smaller in the argon cluster environment than when fully isolated in vacuum. The phase space for coupling with electronic state of lower energy is therefore reduced and the lifetime within the excited potential energy surface is enhanced.

6.3 Dynamics of free and deposited BTF6 and PTF6 molecules in the present experiment *versus* studies in condensed phases

The previous section has shown that when BTF6 and PTF6 are bound to an argon cluster, wavepackets WP_1, WP_2 and WP_3 are not affected in the same way. This is fully consistant with what was anticipated in *Paper I*: these wavepackets are driven by three very different photophysical processes. This three wavepacket picture is consistent also with a recent study of normal dithienylethene molecules in chloroform solution at room temperature, including PTF6, where the photoswitching mechanism was revisited.[5] The mechanistic diagram drawn in Ref. 5 includes the present three wavepacket model. It is actually more complex than that in Fig.8 here because the liquid phase experiment is sensitive to the wavepackets after they left the singlet surface where they have been launched initially. For instance, it is shown that WP_2 and WP_3 go to triplet energy surfaces. The time constants reported in Ref. 5 (τ_1, τ_3, and τ_4) that have a correspondence with those documented here (τ_1, τ_2, τ_3, respectively) are about an order of magnitude smaller than measured here. Beyond that, the excitation energy is not the same in the two works, this might reflect a larger molecular internal temperature in the room temperature liquid phase experiment compared to the present supersonic beam experiment. In spite of these differences, the crucial point shows the three wavepacket picture as intrinsic to n-DTE (and i-DTE) molecules. It applies indeed, whatever the molecule environment: free in the gas phase, bound to an argon cluster or diluted in an organic solvent. Note that Ishibashi et al. reported two time constants, 450 fs and 150 ps, for the excited state dynamics of BTF6 in alkane solutions with a pump excitation at 310 nm.[42] This work was performed before it was clear that in the AP conformer case, an initial wavepacket splits into two sub-wavepackets (WP_1 and WP_2 with the present notations). Hence, the interpretation given in Ref. 42 for the 150 ps time constant could be revisited.

To complete the discussion, let us notice that WP_1 is almost quenched in the BTF6(Ar)$_{\approx 500}$ experiment (small weight$_1$ value in Tab.1) and BTF6 does not photocyclize in the monocrystalline phase.[31] The situation met with PTF6 is different since WP_1 is not quenched in the PTF6(Ar)$_{\approx 500}$ experiment and the photocyclization reaction is observed in monocrystalline PTF6.[31] This might appear as a further evidence that the fate of WP_1 is to promote photocyclisation in BTF6. However cautiously, no definite conclusion can be drawn on the fates of WP_1 and WP_2 in PTF6, whether the photocyclization proceeds only from WP_1 or from both WP_1 and WP_2. The first option was preferred in Ref. 5

7 Conclusions

Real-time excited state dynamics of the open-ring isomer of two normal dithienylethene molecules, 1,2-bis(2-methylbenzo[b]thiophen-3-yl)perfluorocyclopentene (BTF6) and 1,2-bis(2,4-dimethyl-5-phenyl-3-thienyl)-3,3,4,4,5,5,-hexafluoro-1-cyclopentene (PTF6), were explored experimentally with ≈80 fs resolution. These molecules were studied in two different environments: fully isolated in the gas phase or bound to an argon cluster. The experiments were conducted in a molecular beam using the femtochemistry technique. Accordingly, molecules under study were excited electronically near 266 nm and probed by multiphoton ionization near 790 nm using femtosecond laser pulses and an adjustable pump-probe time delay up to 350 ps.

The experimental work was associated with a computational one for the isolated BTF6 molecule. Vertical excitation energies were calculated, indicating that the 266 nm laser excitation populates S_5 and S_6 states. A geometry optimization was performed on the S_5 state indicating that no direct, easy-to-find reactive pathway exists on this surface, which enables switching from the open-ring to the closed-ring isomer. This fits with theoretical works available in the literature, showing that the reaction is promoted by a conical intersection (CI), far from the well of the excited potential energy surface where the reaction is initiated.

When BTF6 and PTF6 molecules were isolated in the gas phase, the experimental work documented their intrinsic dynamics. It mimics a former work of the present group of authors on isolated inverse dithienylethene molecules[6] (labeled *Paper I* throughout the present work). As in *Paper I*, the dynamics can be understood in terms of a three wavepacket model, having one (WP_3) describing the unreactive parallel conformer P of these molecules. WP_3 makes no observable decay at the time scale of the present experiment. The other two wavepackets describe the antiparallel conformer AP. After an electronic excitation, they evolve along two pathways which are essentially independent one from another. One (WP_1) decays rapidly (≈0.5 and ≈1.2 ps for BTF6 and PTF6, respectively), through a CI and reaches a potential energy surface of lower energy where it can no longer be detected. The other (WP_2) is associated with vibronic relaxation within the well of the S_1 excited potential energy surface. The vibronic decay is faster with PTF6 that has more degree of freedom than BTF6 (3-10 ps *versus* 75-80 ps). The behaviour of WP_1 is believed to be ballistic in contrast to WP_2 which describe an energy redistribution within a thermal bath.

When BTF6 and PTF6 molecules are bound to an argon cluster, the same three wavepacket model applies. The interesting and unexpected result shows a perturbation of the WP_1 the ballistic dynamics for BTF6: an obstruction effect by few argon atoms moves a substantial fraction of this wavepacket into vibronic relaxation. No such effect is observed for PTF6. Furthermore, the time constant of vibronic decay is considerably reduced by a factor five. This is interpreted by the smaller initial internal temperature of molecules deposited on argon clusters compared to free molecules.

Acknowledgments

L.P. thanks the ANR for support through the contract ANR-09- JCJC-0090-01 “CHROMADYNE”. Furthermore, we thank the CEA/SLIC staff, in particular Olivier Gobert and Delphine Guillaumet, for technical support.

Notes and references

1 M. Irie, T. Fukaminato, K. Matsuda and S. Kobatake, Chem. Rev., 2014, **114**, 12174–12277.

2 A. Jarota, E. Pastorczak, W. Tawfik, B. Xue, R. Kania, H. Abramczyk and T. Kobayashi, Phys. Chem. Chem. Phys., 2019, **21**, 192–204.

3 H. Sotome, D. Kitagawa, T. Nakahama, S. Ito, S. Kobatake, M. Irie and H. Miyasaka, Phys. Chem. Chem. Phys., 2019, **21**, 8623–8632.

4 Y. Li, J. L. Pérez Lustres, H.-R. Volpp, T. Buckup, T. Kolmar, A. Jäschke and M. Motzkus, Phys. Chem. Chem. Phys., 2018, **20**, 22867–22876.

5 I. Hamdi, G. Buntinx, A. Perrier, O. Devos, N. Jaïdane, S. Delbaere, A. K. Tiwari, J. Dubois, M. Takeshita, Y. Wada and S. Aloïse, Phys. Chem. Chem. Phys., 2016, **18**, 28091–28100.

6 A. Lietard, G. Piani, L. Poisson, B. Soep, J.-M. Mestdagh, S. Aloïse, A. Perrier, D. Jacquemin and M. Takeshita, Phys. Chem. Chem. Phys., 2014, **16**, 22262–22272.

7 L. Poisson, K. D. Raffael, B. Soep, J. M. Mestdagh and G. Buntinx, J. Am. Chem. Soc., 2006, **128**, 3169–3178.

8 L. Poisson, P. Roubin, S. Coussan, B. Soep and J. M. Mestdagh, J. Am. Chem. Soc., 2008, **130**, 2974–2983.

9 J.-M. Mestdagh and L. Poisson, ChemPhysChem, 2020, **21**, 2605–2613.

10 A. Lietard, G. Gallician, J. Tan, M. A. Gaveau, M. Briant, B. Soep, J. M. Mestdagh and L. Poisson, Mol. Phys., 2021, **119**, e1737743.

11 L. Poisson, E. Gloaguen, J.-M. Mestdagh, B. Soep, A. Gonzalez and M. Chergui, J. Phys. Chem. A, 2008, **112**, 9200–9210.

12 S. Awali, L. Poisson, B. Soep, M.-A. Gaveau, M. Briant, C. Pothier, J.-M. Mestdagh, M. B. E. H. Rhouma, M. Hochlaf, V. Mazet and S. Faisan, Phys. Chem. Chem. Phys., 2014, **16**, 516.

13 S. Awali, J.-M. Mestdagh, M.-A. Gaveau, M. Briant, B. Soep, V. Mazet and L. Poisson, J. Phys. Chem. A, 2021, **125**, 4341–4351.

14 S. Awali, M. A. Gaveau, M. Briant, J. M. Mestdagh, B. Soep, O. Gobert, R. Maksimenka and L. Poisson, Phys. Chem. Chem. Phys., 2016, **18**, 32378 – 32386.

15 J. Farges, M. F. de Feraudy, B. Raoult and G. Torchet, J. Chem. Phys., 1986, **84**, 3491–3501.

16 S. Shim, I. Eom, T. Joo, E. Kim and K. S. Kim, J. Phys. Chem. A, 2007, **111**, 8910–8917.

17 S. Shim, T. Joo, S. C. Bae, K. S. Kim and E. Kim, J. Phys. Chem. A, 2003, **107**, 8106–8110.

18 M. Irie, T. Lifka, S. Kobatake and N. Kato, J. Am. Chem. Soc, 2000, **122**, 4871–4876.

19 A. Stolow, Annu. Rev. Phys. Chem., 2003, **54**, 89–119.

20 A. Stolow, A. E. Bragg and D. M. Neumark, Chem. Rev., 2004, **104**, 1719–1757.

21 G. A. Garcia, L. Nahon and I. Powis, Rev. Sci. Instrum., 2004, **75**, 4989–4996.

22 S. Awali, J.-M. Mestdagh, M.-A. Gaveau, M. Briant, B. Soep, V. Mazet and L. Poisson, J. Phys. Chem. A, 2021, **125**, 4341–4351.

23 P. M. Felker and A. H. Zewail, J. Chem. Phys., 1987, **86**, 2460–2482.

24 Anonymous, Turbomole V6.3 2011, a Development of University of Karlsruhe and Forschungszentrum Karlsruhe Gmbh, 1989-2007, Turbomole Gmbh, since 2007; Available from Http://Www.Turbomole.Com.

25 S. Kobatake, T. Yamada, K. Uchida, N. Kato and M. Irie, J. Am. Chem. Soc, 1999, **121**, 2380–2386.

26 R. Pollet and V. Brenner, Theoretical Chemistry Accounts, 2008, **121**, 307–312.

27 P. D. Patel and A. E. Masunov, J. Phys. Chem. A, 2009, **113**, 8409–8414.

28 S. Grimme, J. Antony, S. Ehrlich and H. Krieg, J. Chem. Phys., 2010, **132**, 154104.

29 A. Röder, J. Petersen, K. Issler, I. Fischer, R. Mitric and L. Poisson, J. Phys. Chem. A, 2019, **123**, 10643–10662.

30 Y. Asano, A. Murakami, T. Kobayashi, S. Kobatake, M. Irie, S. Yabushita and S. Nakamura, Journal of Molecular Structure-Theochem, 2003, **625**, 227–234.

31 S. Kobatake, K. Uchida, E. Tsuchida and M. Irie, Chem. Commun., 2002, 2804–2805.

32 K. Uchida, E. Tsuchida, Y. Aoi, S. Nakamura and M. Irie, Chemistry Letters, 1999, **28**, 63–64.

33 M. Irie, K. Uchida, T. Eriguchi and H. Tsuzuki, Chemistry Letters, 1995, 899–900.

34 H. Miyasaka, T. Nobuto, M. Murakami, A. Itaya, N. Tamai and M. Irie, J. Phys. Chem. A, 2002, **106**, 8096–8102.

35 M. Boggio-Pasqua, M. Ravaglia, M. J. Bearpark, M. Garavelli and M. A. Robb, J. Phys. Chem. A, 2003, **107**, 11139–11152.

36 A. Perrier, S. Aloïse, M. Olivucci and D. Jacquemin, J. Phys. Chem. Lett., 2013, **4**, 2190–2196.

37 A. Röder, A. Humeniuk, J. Giegerich, I. Fischer, L. Poisson and R. Mitric, Phys. Chem. Chem. Phys., 2017, **19**, 12365–12374.

38 A. Röder, K. Issler, L. Poisson, A. Humeniuk, M. Wohlgemuth, M. Comte, F. Lepetit, I. Fischer, R. Mitric and J. Petersen, J. Chem. Phys., 2017, **147**, 013902.

39 K. Shibata, K. Muto, S. Kobatake and M. Irie, J. Phys. Chem. A, 2001, **106**, 209–214.

40 H. Jean-Ruel, R. R. Cooney, M. Gao, C. Lu, M. A. Kochman, C. A. Morrison and R. J. D. Miller, J. Phys. Chem. A, 2011, **115**, 13158–13168.

41 L. Poisson, R. Maksimenska, B. Soep, J. M. Mestdagh, D. H. Parker, M. Nsangou and M. Hochlaf, J. Phys. Chem. A, 2010, **114**, 3313–3319.

42 Y. Ishibashi, M. Fujiwara, T. Umesato, H. Saito, S. Kobatake, M. Irie and H. Miyasaka, J. Phys. Chem. C, 2011, **115**, 4265–4272.